iScience

CellPress
OPEN ACCESS

Perspective

Cryo-EM for battery materials and interfaces: Workflow, achievements, and perspectives

Suting Weng,[1,2] Yejing Li,[1,*] and Xuefeng Wang[1,2,3,*]

SUMMARY

The emerging cryogenic electron microscopy (cryo-EM) has demonstrated its power and essential role in probing the beam-sensitive battery materials and delivering new insights. With the increasing interest in cryo-EM for battery materials and interfaces, herein we provide the strategies of obtaining fresh and native structural information with minimal artifacts, including sample preparation, transferring, imaging, and data interpretation. We summarize the recent achievements enabled by cryo-EM and point out some unsolved/potential questions in terms of the bulk materials, solid-solid interface, and solid-liquid interfaces of batteries. Finally, we conclude with perspectives on the future developments and applications of cryo-EM in battery materials and interfaces.

INTRODUCTION

Lithium-ion batteries have been commercialized for three decades since 1991. However, some critical challenges such as the nature of solid electrolyte interphase (SEI) have been pursued to address due to the technical limits to characterize and diagnose the battery materials and interfaces especially at the atomic scale (Banerjee et al., 2020; Liu et al., 2019a; Verma et al., 2010; Wu et al., 2020). This issue becomes more severe when light-element (non-transition metals) and/or nanoscale materials are used for the next-generation high-energy batteries, such as lithium-sulfur (Li-S) batteries, Li-air batteries, and solid-state batteries (Lin et al., 2017; Liu et al., 2018a; Xin et al., 2017).

The emerging cryogenic electron microscopy (cryo-EM) has been demonstrated to have power and an essential role in probing the beam-sensitive battery materials and delivering many new insights (Wang et al., 2017, 2018). We summarized the literature associated with cryo-EM in the recent 20 years through the Web of Science and found that the interest in cryo-EM was gradually increased and exploded after 2015 (Figure 1A). Its application in the batteries field raised growing attention when it was used to disclose the nanostructure of the electrochemically deposited Li metal (EDLi) in 2017 (Figure 1A) (Li et al., 2017; Wang et al., 2017). The success of the cryo-EM for the batteries materials mainly lies in the reduced reactivity and enhanced stability of samples enabled by cryogenic temperature and lowered electron dose for processing and imaging (Figure 1B). The schematic working principles of cryo-EMs including cryo-focus ion beam (cryo-FIB) and cryo-transmission electron microscopy (cryo-TEM) are displayed in Figures 1C and 1D, respectively.

Several review articles related to the application of cryo-EM for batteries have been published in the past few years (Ju et al., 2021b; Li et al., 2020a; Liu et al., 2021b; Ren et al., 2020; Wang et al., 2018; Wu et al., 2021; Zhang et al., 2021c), which cover the achievements from some specific topics or groups. When cryo-EM is becoming an essential technique in the battery community, a routine workflow customized for battery materials and interfaces is highly needed to guarantee native and fresh information from samples, which is rarely involved in the previous literature. Therefore, this perspective will first provide the state-of-the-art workflow of cryo-EM for different battery materials and interfaces, including sample preparation, transferring, imaging, and data analysis. Recent achievements by using cryo-EM will be summarized, and the remaining/potential questions which probably need cryo-EM, will be exampled for the benefit of future battery research. Last but not least, the emerging analytical technologies are expected to couple with cryo-EM to develop a more efficient, powerful, intelligent, and integrated technique for materials science.

[1]Laboratory for Advanced Materials and Electron Microscopy, Institute of Physics, Chinese Academy of Sciences, Beijing 100190, China

[2]School of Physical Sciences, University of Chinese Academy of Sciences, Beijing 100049, China

[3]Tianmu Lake Institute of Advanced Energy Storage Technologies Co. Ltd., Liyang, Jiangsu 213300, China

*Correspondence: liyejing26@gmail.com (Y.L.), wxf@iphy.ac.cn (X.W.)

https://doi.org/10.1016/j.isci.2021.103402

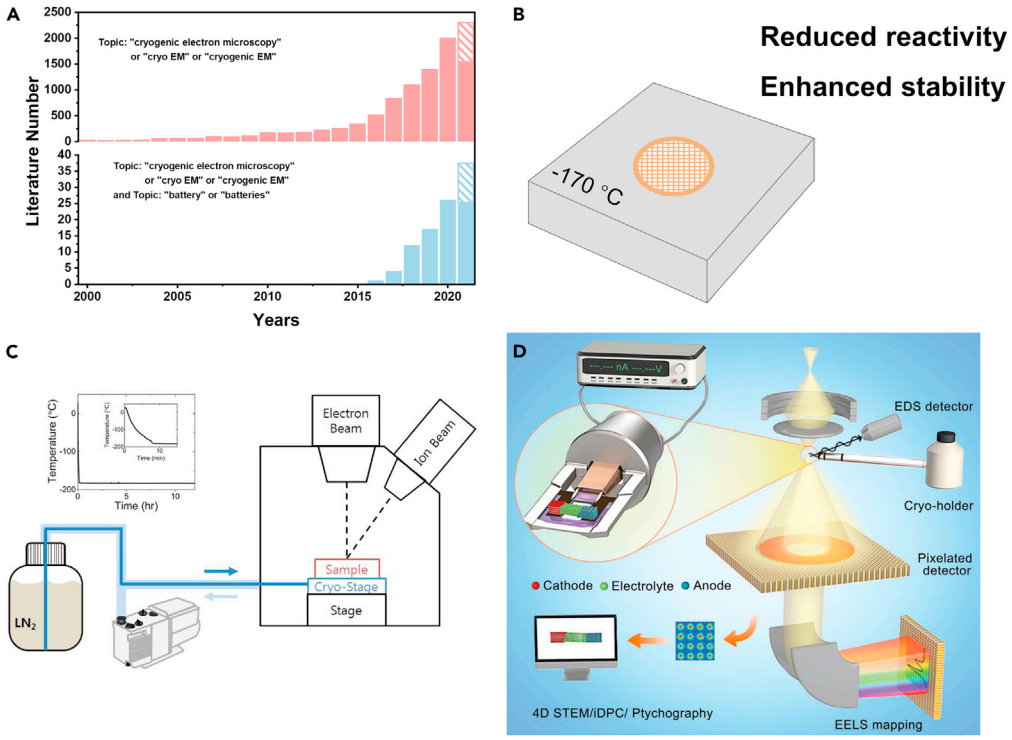

Figure 1. Article publishing trends and related technologies of cryo-EM

(A) Summarized literature number as a function of years. The dashed box in Figure 1A corresponds to the estimated literature number to be published in the rest of 2021. The state-of-the-art works on cryo-EM for battery materials and interfaces are summarized in Table S1.

(B) Benefits of cryogenic temperature.

(C and D) Schematic diagram of cryo-FIB (C) (Lee et al., 2019) and cryo-TEM (D) (Zhang et al., 2020b). Copyright © 2019, American Chemical Society and Copyright © 2020, Wiley, respectively.

WORKFLOW OF CRYO-EM

To obtain the fresh and native structural information of the battery materials and interfaces with minimal artifacts, it is critical to minimize the contamination, damage, and misleading analysis during sample preparation, transferring, imaging, and data interpretation. Based on the physical properties of samples, a routine method is provided in Figure 2 as guidance for newcomers (Wang et al., 2018).

Sample preparation: Conventional method by directly dispersing the particles on the TEM grid works for most solid particles and solid-solid interfaces. It is cautious to apply ultrasonic treatment for better dispersion because the high-energy wave may destroy the fragile samples, such as Li metal and SEI/cathode electrolyte interphase (CEI). For those large particles and buried solid-solid interface, cryo-FIB or cryo-ultramicrotomy (Chen, 2021) is suggested to thin the sample. If possible, placing a TEM grid in the batteries as a part of the current collector is a smart way to achieve a sample approaching its real electrochemical states, for example, directly plating Li/Na metal on it (Wang et al., 2018). Special attention should be paid when dealing with the fragile grid to avoid over-washing or mechanical damage.

Solid-liquid interfaces are prevalent during materials synthesis, electrode fabrication, and battery operation, which are important but rarely explored owing to difficulties in handling the liquid phase. In this regard, inspired by the biologic community, the liquid phase will become a glassy phase during plunge/rapid freezing. Thus the previous solid-liquid interface is converted to the solid-solid interface while maintaining their contact and interplay (Zachman et al., 2020). By this method, Zachman et al. obtained the interface between Li metal and liquid electrolyte for scanning transmission electron microscope (STEM) imaging (Zachman et al., 2018). With this successful demonstration, more interesting works are on the way to revealing the mystery of various solid-liquid interfaces in batteries.

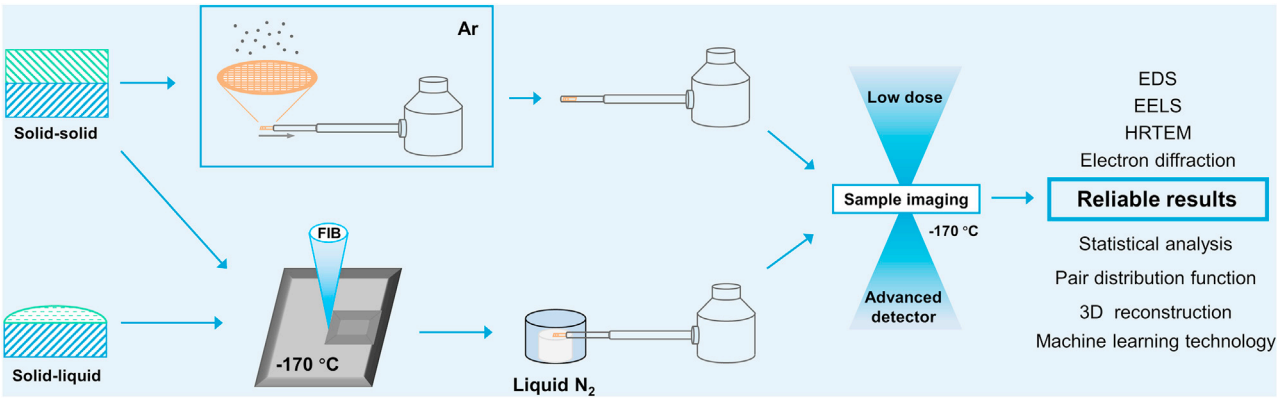

Figure 2. Routine method of cryo-EM for different samples.

Transferring: Once the sample is prepared, it is important to guarantee a safe transfer before inserting it into the TEM chamber especially for those air-sensitive battery materials. Specially designed TEM holders are preferred that enable cryo transfer, or vacuum/sealing transfer, which have been commercialized in recent years.

Imaging: Cryo-EM has the same capability as conventional electron microscopy and shows its unique merits for beam-sensitive materials. Therefore, morphology, crystalline structure (high-resolution transmission electron microscopy [HRTEM]), electronic structure (electron energy loss spectroscopy [EELS]), and elemental distribution (energy dispersive spectroscopy [EDS]), etc. can be obtained from cryo-EM with minimal artifacts (Li et al., 2017; Wang et al., 2017). For beam-sensitive samples, high electron beam dose causes the materials to melt, shrink, and sublime, whereas low dose leads to poor signal-to-noise ratio (SNR). Therefore, it is key to find a trade-off between dose and SNR for each sample. Experimentally, we should start with an ultralow dose, then gradually increase the dose to improve the SNR of the image without damaging the sample, and finally determine the appropriate electron dose for different samples. To improve the SNR, advanced cameras such as direct electron detection cameras enable to image faster, correct drift, and raise the detective quantum efficiency.

Data analysis: Since TEM is a technique sensitive to local regions, how to report a reliable and representative result becomes a great challenge. In this sense, statistical analysis is highly suggested especially when the sample is heterogenetic (Cheng et al., 2020a; Fang et al., 2019; Li et al., 2017; Wang et al., 2020b; Yang et al., 2021b). The workflow of statistical analysis (Figure 3A) includes collecting data at random regions, identifying the information of interest such as the phases and distribution from all the acquired images, and finally counting their frequency to obtain the statistical analysis results. Figures 3B–3E show several applications of statistical analysis. Wang et al. (2020b) identified ~100 random lithium dendrites and correlated the crystallinity of EDLi with the deposition rate. Since SEI is inhomogeneous in its component and distribution, it is hard to make a conclusion based on a single image, which may be misleading (Cheng et al., 2020a; Yang et al., 2021b). Statistical analysis provides more representative and convincing results, which in turn gives more work for the data collection and analysis.

INSIGHTS AND PERSPECTIVE FROM CRYO-EM FOR BATTERY

The past four years witnessed increasing attention and progress from cryo-EM for the battery materials and interfaces, which are illustrated in Table S1. In this section, we summarize these achievements and point out some remaining/potential questions in need of cryo-EM in terms of the bulk materials, solid-solid interfaces, and solid-liquid interfaces.

Bulk materials

Electrodes: Electrode fabrication is important to construct an electronic network and fulfill the capacity of active materials, which involves powder mixing, slurry casting, and drying. The changes in the microstructure of the electrode during drying or cycling are rarely explored. FIB coupled with scanning electron microscopy (SEM) enables visualization of large (>100 μm) regions and provides structural/morphology

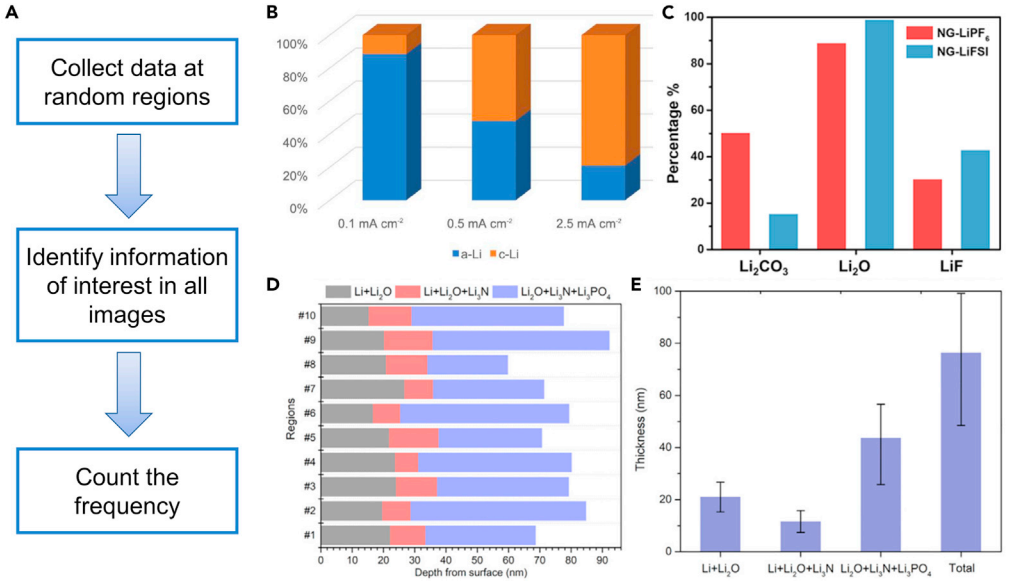

Figure 3. Statistical analysis of TEM images

(A) The steps of statistical analysis.

(B–E) Application of statistical analysis in the literature. (B) Statistical analysis on the possibility/distribution of amorphous-Li (a-Li) and crystalline-Li (c-Li) in different current densities (Wang et al., 2020b). Copyright © 2020, Springer Nature. (C) The percentages (relative frequencies of being found) of the detected Li_2CO_3, Li_2O, and LiF in different electrolytes (Yang et al., 2021b). Copyright © 2021, American Chemical Society. Depth distribution (D) and averaged thickness (E) of different layers within the Li/LiPON interphase extracted from 10 different regions (Cheng et al., 2020a). Copyright © 2020, Elsevier.

information at the electrode level. Meanwhile, cryogenic treatment can solidify the liquid phases and maintain structural integrity. Therefore, by using cryo-BIB (broad ion beam)-SEM, Jaiser et al. explored the electrode change during drying (Figure 4A) (Jaiser et al., 2017). The results show that the electrode film is gradually shrinking from 104 to 96 μm, then to 69 μm after continuous solvent evaporation and finally reaches 61 μm (Figures 4B–4E). The distribution of graphite particles, liquid phase, binders, and pores is visible especially in the EDS mappings (Figures 4F–4G). After collecting a series of high-resolution cross-sectional images, Lee et al. (2019) created a three-dimensional (3D) reconstruction of the EDLi by cryo-FIB-SEM, from which the size, shape, and packing density of Li and distribution of voids can be quantitively measured and thus correlated with the electrochemical performance. This method is expected to extend to probe the electrode change during cycling with liquid or solid electrolytes, uncovering the microstructure evolution of different components and their interfaces at the electrode level.

Active materials: The atomic structure of active materials regulates their capability and kinetic for ion storage and diffusion. Probing the structure evolution of beam-sensitive battery materials like Li metal is challenging but critical to understand their electrochemical behaviors. The nanostructure of materials in the electrode can be revealed by cryo-TEM (Lin et al., 2019). Li et al. (2017) observed that the Li dendrites prefer to grow along <111> in the carbonate-based electrolytes, which can be suppressed by interphase engineering derived from the eggshell (Ju et al., 2020). The crystallinity evolution of the Li metal as a function of deposition time and the rate was investigated by Wang et al. (Figure 5) (Wang et al., 2020b). They discovered the disorder-to-order phase transition during cycling: most of EDLi is amorphous at the initial nucleation stage (5 min in Figures 5A and 5D), especially at a lower current density (0.1 mA cm^{-2}, Figures 5G and 5J). The critical size to form a crystalline Li cluster is about 5 nm (Figure 5B). Amorphous-rich Li is proved beneficial to reduce the dendritic growth and enhance electrochemical reversibility. Besides tuning current density and electrolyte (Wang et al., 2020b), amorphous Li clusters can be obtained by introducing hetero-atom-activating electronegative sites on the current collector and thus improving the cycling performance (Huang et al., 2021). Although these works enrich the understanding of the Li growth, much work is still needed to uncover the behaviors of Li metal at different conditions, such as varied electrolytes, temperature, and pressures.

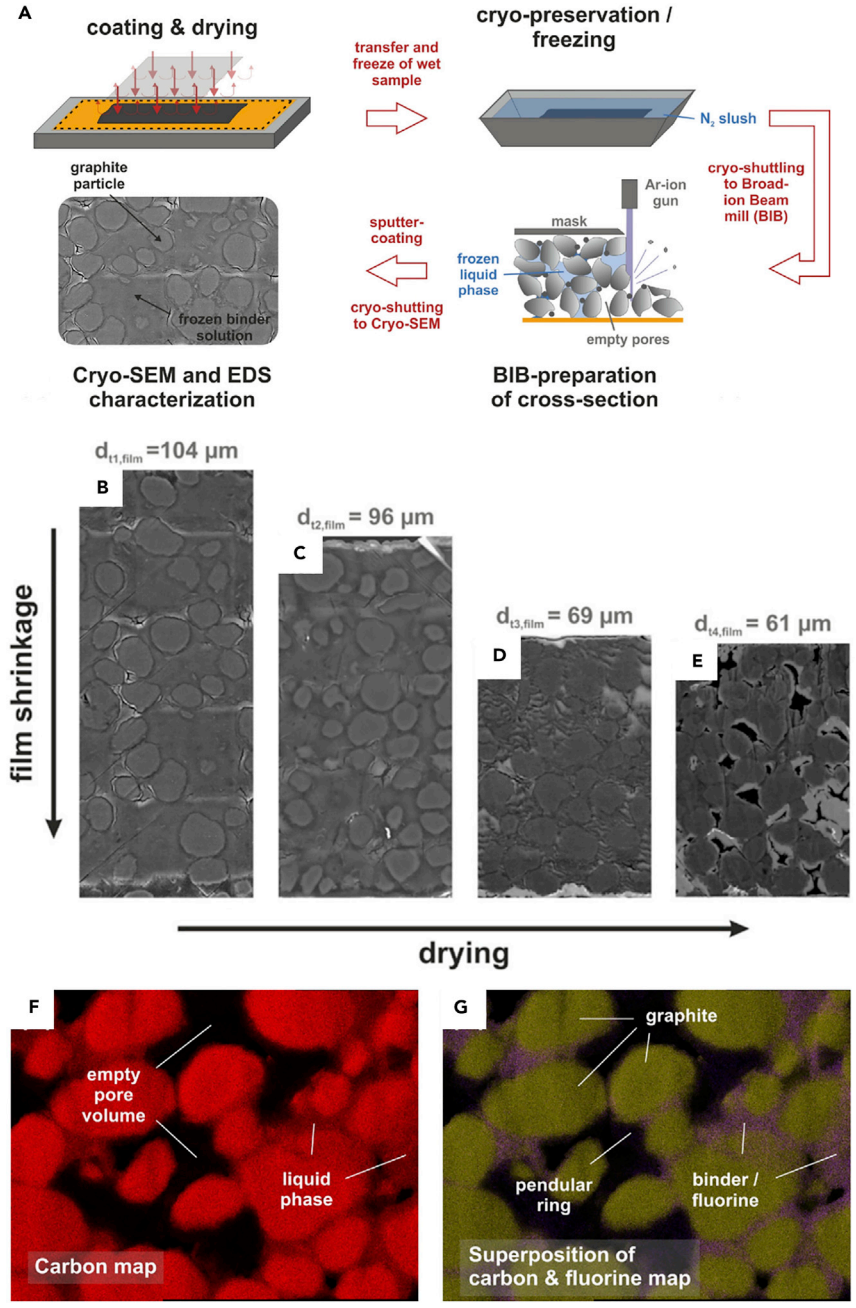

Figure 4. Microstructure evolution of graphite electrode films during drying by cryo-BIB (broad ion beam)-SEM

(A) Illustration of the sample preparation procedure.

(B–E) SEM micrographs of electrode films at 8.0 (B), 15.1 (C), 37.4 (D), and 55.7 s (E).

(F and G) EDS mappings of carbon (F) and superposition of the carbon and the fluorine (G) in a drying electrode film (Jaiser et al., 2017). Copyright © 2017, Elsevier.

Besides Li metal, many other battery materials are sensitive to the beam, including oxides, sulfides, and other anode materials (Soulmi et al., 2017; Yang et al., 2021a). Li-rich oxides and high-Ni oxides are subjected to surface reconstruction under continuous electron beam radiation (Gao et al., 2020), suggesting the potential need for cryo-TEM to reduce the artifacts caused by the beam (Tyukalova et al., 2021). He et al. tracked the morphology evolution of Si nanowire during the long-term cycles and found that it is gradually bent and becomes porous after 100 cycles, which seriously degrades its cycling

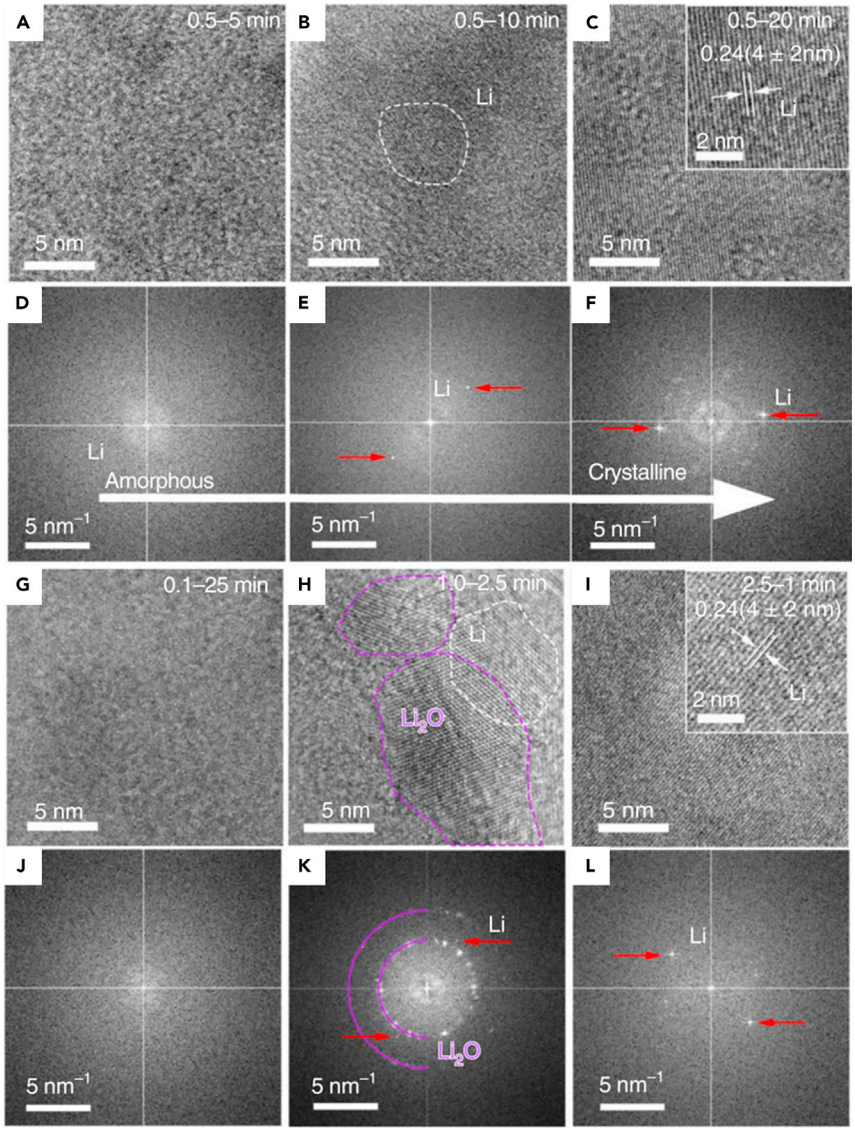

Figure 5. Nanostructure evolution of Li deposit as a function of deposition time and rate

(A–L) Cryo-TEM images (A–C and G–I) and their corresponding fast Fourier transform patterns (D–F and J–L) of the Li deposits at 0.5 mA cm^{-2} for 5 (A and D), 10 (B and E), and 20 min (C and F); 0.1 mA cm^{-2} for 25 min (G and J); 1.0 mA cm^{-2} for 2.5 min (H and K); and 2.5 mA cm^{-2} for 1.0 min (I and L). The images with the Li metal lattice and the characteristic bright diffraction spots highlighted by the red arrows are from the (110) plane of Li metal (Wang et al., 2020b). Copyright © 2020, Springer Nature.

performance (Figure 6A) (He et al., 2021). Elemental S is volatile in the high-vacuum TEM, which can be alleviated at cryogenic temperature, providing a way to probe the nanostructure of S-containing materials, such as Fe_3O_4/S composite and CoS_2/S composite (Levin et al., 2017; Liu et al., 2018d; Zhang et al., 2018, 2019). Yu et al. observed the phase separation of Mo and Li_2S in the fully lithiated MoS_2 and suggested the Mo and S migrating independently after Mo-S bonds rupture (Figures 6B and 6C) (Yu et al., 2019). Sulfide solid electrolytes are also beam sensitive (Li et al., 2020b; Song et al., 2020). The uniform distribution of crystalline β-Li_3PS_4 in amorphous polyethylene sulfide was confirmed by cryo-TEM; the composite shows a high conductivity of 2×10^{-5} S cm^{-1} at room temperature (Figure 6D) (Li et al., 2020b). Therefore, in the future, cryo-TEM will be highly wanted to probe the nanostructure of the various cathode, electrolyte, and anode materials; uncover their working principles; and correlate with the electrochemical performance.

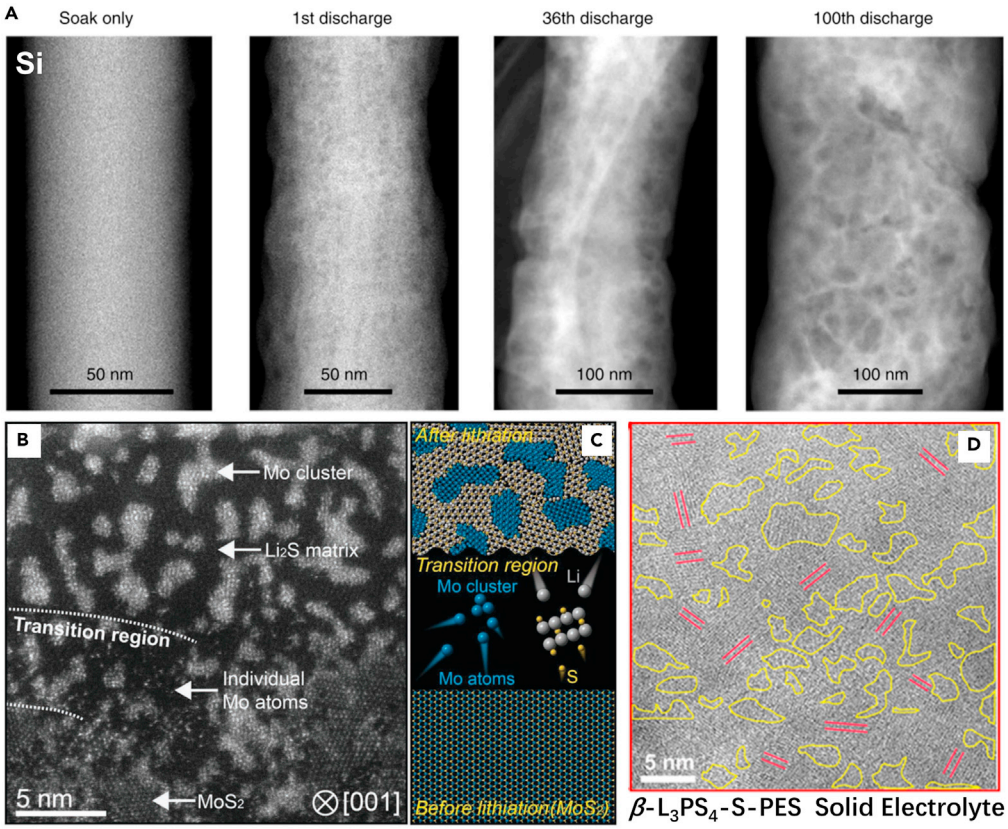

Figure 6. Cryo-EM images on the bulk battery materials

(A) Cryo-STEM-HAADF images of the Si nanowires at different cycles. The "soak only" sample was prepared by soaking fresh Si nanowire in the electrolyte without charge/discharge (He et al., 2021). Copyright © 2021, Springer Nature.

(B) Annular dark-field cryo-STEM image of the partially lithiated MoS_2 monolayer (Yu et al., 2019).

(C) Schematic illustration of the conversion reaction in MoS_2 monolayer (Yu et al., 2019). Copyright © 2019, Wiley.

(D) Cryo-TEM image for the nanostructure of the β-Li_3PS_4-S-PES solid electrolyte. Areas with yellow circles and red lines correspond to the amorphous and crystalline species, respectively (Li et al., 2020b). Copyright © 2020, American Chemical Society.

Solid-solid interfaces

Solid-solid interfaces regulate the charge transfer and ion diffusion in the batteries, determining the reaction rate and safety of the batteries. Of particular interest are the SEIs, CEIs, and the interfaces in the solid-state batteries (Alvarado et al., 2019; Han et al., 2020; Li et al., 2018; Liu et al., 2018b; Thenuwara et al., 2019; Vilá et al., 2020; Xu et al., 2020b). The passivation layers formed by the decomposition of the electrolyte on the surface of the anode during the charge and discharge are called SEIs and those formed on the cathode are referred to CEIs.

Solid electrolyte interphases: SEI is regarded as the most important but the least understood part in batteries. There is no consensus on the composition, content, distribution, evolution of SEI as well as its correlation with the ionic conductivity and mechanical property (Han et al., 2021a; Ju et al., 2021a; Liu et al., 2019b, 2021a, 2021c; Yuan et al., 2020a). Two typical models that are mosaic structure (Peled et al., 1997) and multilayer structure (Aurbach et al., 1994) were proposed and observed in different electrolytes (Han et al., 2021c; Li et al., 2017, 2021; Liu et al., 2018e; Zhang et al., 2020a). In mosaic structure, inorganic nanocrystals such as Li_2O, LiF, and Li_2CO_3 are embedded in the amorphous organic matrix and their components, content, and distribution vary at different cell conditions (Xu et al., 2020a; Yuan et al., 2020b). Especially, the attractive fluorinated interphase has been proved beneficial in improving the electrochemical performance of Li metal while the underneath working principle is controversial (Sheng et al., 2020b; Yuan et al., 2020b, 2021; Zhang et al., 2021a). Most references proved the presence and increased content

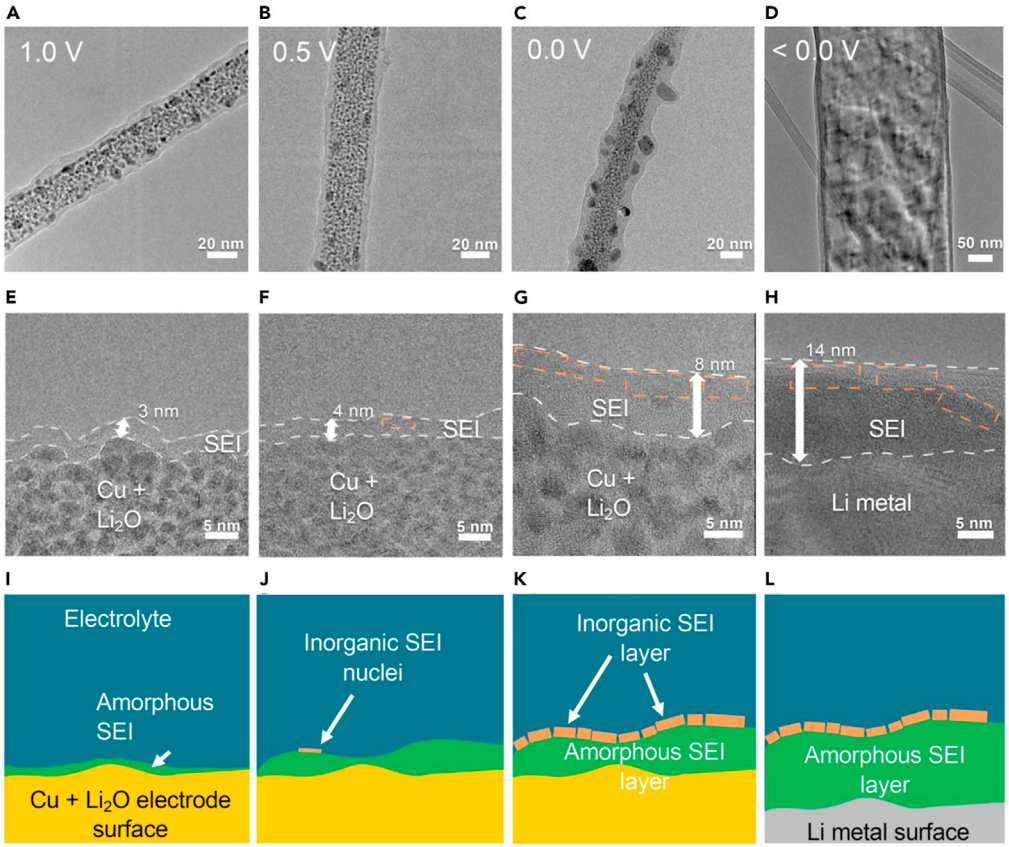

Figure 7. Structural evolution of SEI on CuO nanowires

(A–L) Low-magnification images (A–D), high-magnification images (E–H), and schematic diagrams (I–L) of the SEI formed on CuO and Li at different potentials (Huang et al., 2019c). Copyright © 2019, American Chemical Society.

of LiF in SEI by X-ray photoelectron spectroscopy, whereas Yuan et al. (2021) and Huang et al. (2020) observed the individual LiF particles larger than 50 nm outside of the compact SEI. It is hard to imagine how these large particles interact with Li deposition and improve the electrochemical reversibility of Li metal. Moreover, LiF itself will limit the transport of Li ions theoretically owing to its electronic and ionic insulation. Therefore, it is still challenging to reveal the nature of the SEI and its function in regulating the ionic and mechanical properties of the battery interphase.

The evolution of SEI as a function of voltage (Huang et al., 2019c, 2019d), cycle number (He et al., 2021), or temperature (Wang et al., 2019b; Yan et al., 2019) is critical to the cycling performance of batteries. Huang et al. used CuO nanowire as the substrate and probed the SEI at different voltages. When the cell was discharged from 1.0 to 0 V and even lower, the SEI on the nanowire gradually becomes thicker (from 3 nm at 1.0 V to 8 nm at 0 V, then to 14 nm on the plated Li) and more crystalline particles form and distribute inhomogeneously (Figure 7) (Huang et al., 2019c). Note that these observations are specific to the SEI on the CuO rather than a general phenomenon extended for other substrates considering their potential catalytic effect on SEI formation (Huang et al., 2019d). After multiple cycles, SEI was found to accumulate and wrap the active material, resulting in the "dead" Li and capacity loss (Fang et al., 2019; He et al., 2021; Jin et al., 2021). Given the insufficient understanding of the SEI landscape, a lot of work is going to probe the dynamic changes of SEI under different conditions.

SEI varies at different substrates and electrolytes (Dong et al., 2021b; Huang et al., 2019a; Huang et al., 2019b; Huang et al., 2019d; Ihsan-Ul-Haq et al., 2020; Wang et al., 2019a). A silk fibroin-derived current collector leads to spherical Li deposits with a uniform SEI on the surface (Figures 8A and 8B) (Zhang et al., 2020a). When the Li was deposited on graphite, Yang et al. found that the FSI^- anion contributes to forming

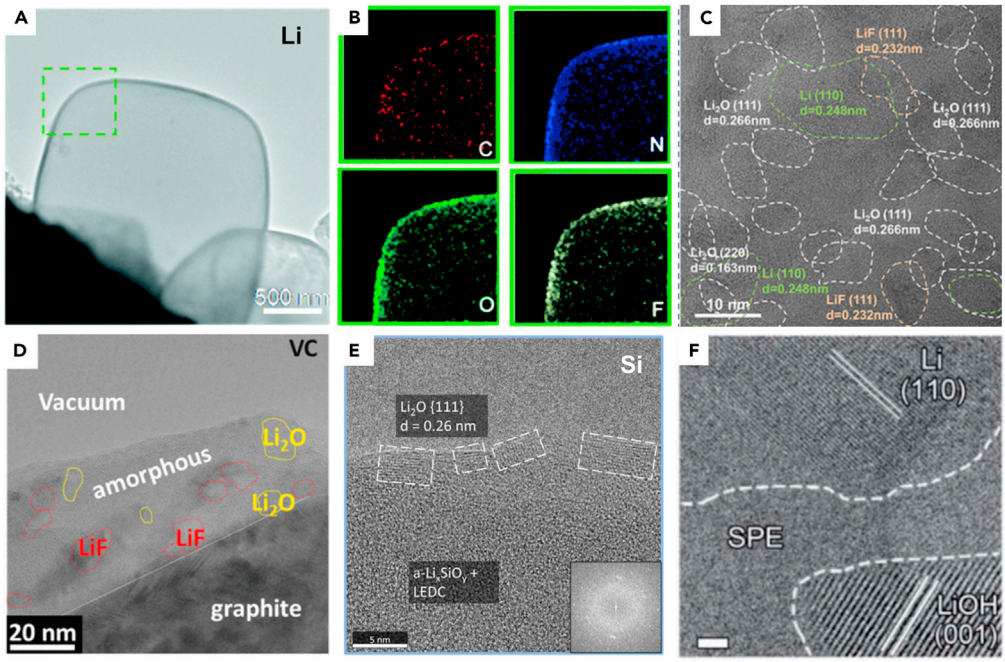

Figure 8. Cryo-TEM image of SEI on different anode materials

(A) Morphologies of Li plated on a bare Cu grid in the silk fibroin-Li structure (Zhang et al., 2020a).

(B) Corresponding elemental mapping images of C, N, O, and F (Zhang et al., 2020a). Copyright © 2020, The Royal Society of Chemistry.

(C) SEI of lithium deposited on graphite (Yang et al., 2021b). Copyright © 2021, American Chemical Society.

(D) SEI on graphite with vinylene carbonate (VC) as the additive (Han et al., 2021b). Copyright © 2021, The Royal Society of Chemistry.

(E) SEI of lithiated Si nanowire (Huang et al., 2019d). Copyright © 2019, Elsevier.

(F) SEI of EDLi in contact with solid polymer electrolytes. Scale bars, 2 nm (Sheng et al., 2020a). Copyright © 2020, The Royal Society of Chemistry.

a more compact and stable SEI (Figure 8C) compared with PF_6^- (Yang et al., 2021b). Electrolyte additives such as VC are preferentially decomposed to form Li_2O- and LiF-rich SEI on the graphite surface, preventing the subsequent graphite exfoliation (Figure 8D) (Han et al., 2021b). Huang et al. visualized the repeated forming and vanishing of Li_2O in the SEI of the Si nanowire during discharge and charge, indicating the high instability of the Si SEI (Figure 8E) (Huang et al., 2019d). At the Li/PEO-based solid polymer electrolyte, a mosaic-structure SEI is present and consists of the organic component and inorganic species, such as LiOH (Figure 8F), which increases the resistance of the solid batteries (Sheng et al., 2020a). Besides Li-ion batteries, the SEI on the Na ion and K ion batteries were also characterized by the cryo-TEM, and its property is closely related to the electrochemical performance (Han et al., 2021c; Le et al., 2020; Sun et al., 2019). For example, Ihsan-Ul-Haq et al. found a uniform and thin SEI (~35.7 nm) formed on the amorphous Sb_2Se_3 while an uneven SEI film with its thickness up to ~71.8 nm was present on the crystalline Sb_2Se_3 (Ihsan-Ul-Haq et al., 2021b). A thin and compact SEI is beneficial to suppress the unwanted side reactions with the electrolyte and enables fast Na^+ ion transport across it (Mubarak et al., 2021).

Cathode electrolyte interphases: Compared with SEI, CEI is less explored since it is thin and shadowed by the surface construction and bulk structural change of cathode materials (Alvarado et al., 2018; Zhang et al., 2021d). Alvarado et al. observed a thin but uniform CEI of about 0.6 nm on the cycled $LiNi_{0.5}Mn_{1.5}O_4$ (LNMO) with the sulfone-based electrolyte, whereas it is unevenly distributed with the conventional carbonate electrolyte (Alvarado et al., 2018). Zhang et al. did not find an obvious CEI on the cycled $LiNi_{0.5}Co_{0.2}Mn_{0.3}O_2$ (NMC532) for multiple particles and suggested the highly heterogeneous nature or instability of CEI (Zhang et al., 2021d). On the contrary, a thick CEI of about 27 nm was visualized on the surface of sulfurized polyacrylonitrile with 4M LiTFSI, which is dominated by LiF and $LiNO_2$ and enables to suppress the formation of soluble polysulfides (Xing et al., 2019). A thin CEI (~1.1 nm) was also found

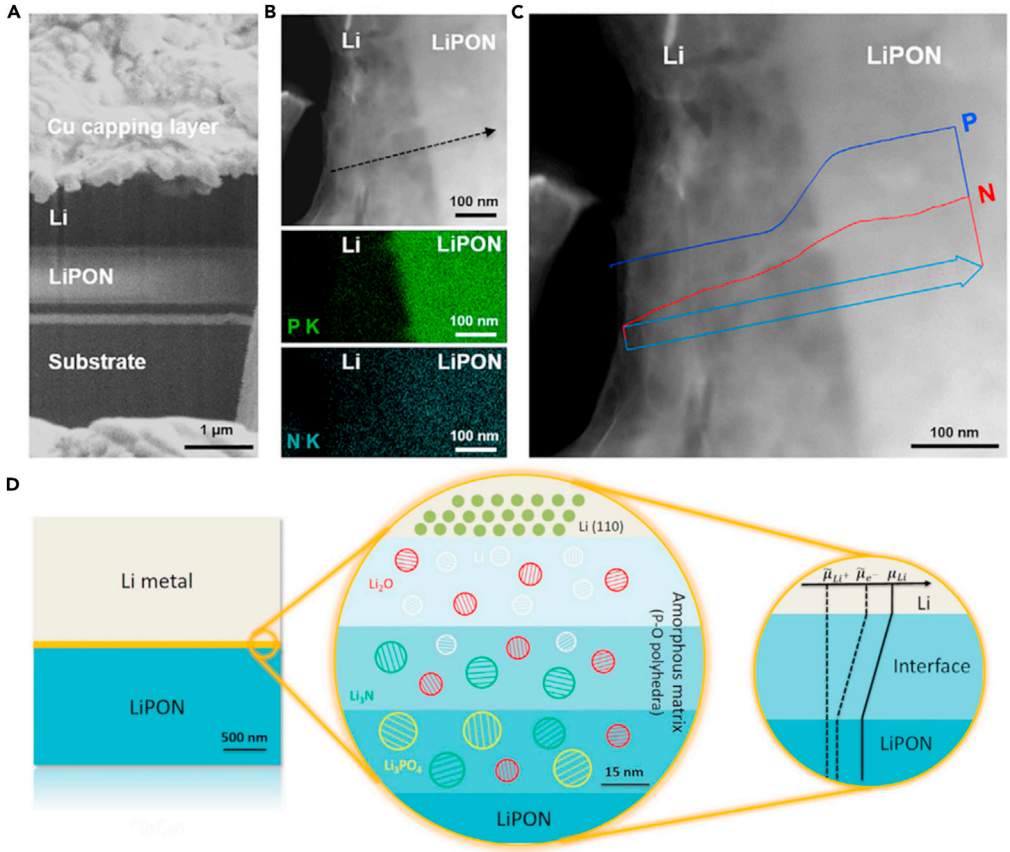

Figure 9. The interface of Li and LiPON by cryo-FIB

(A) Cross-sectional image of the Li/LiPON sample.

(B) EDS mapping results of P and N signals.

(C) EDS line scan of P and N signals (counts per second) along the black dashed arrow in (B).

(D) Li/LiPON multilayered interphase schematic (Cheng et al., 2020a). Copyright © 2020, Elsevier.

on the $Na_3V_2(PO_4)_3$/C particle, which may reduce the interface impedance (Ihsan-Ul-Haq et al., 2021a). With the increasing attention on the importance of CEI, cryo-TEM provides a powerful technique to reveal the nanostructure of CEI and its non-negligible influence on cell performance and safety.

Interfaces in all-solid-state batteries: The pursuit of higher-energy and safer batteries pushes the rapid development of all-solid-state batteries (ASSBs), in which severe interfacial reactions and resistances deteriorate the cycling and rate performance of ASSBs. Probing the interfaces inside the ASSBs is challenging not only on harvesting the buried interface but also on characterizing the fragile and beam-sensitive interphases. A combination of cryo-FIB and cryo-TEM provides an effective way to alleviate these issues (Cheng et al., 2020a; Cui et al., 2020; Zheng et al., 2020). Cui et al. (2020) and Zheng et al. (2020) performed a 3D reconstruction of the Li/LLZO interface from FIB sectioning tomography. Cheng et al. (2020a) demonstrated this methodology with the Li/LiPON interface and applied HRTEM, EDS, and EELS to analyze the interphases (Figure 9). The Li/LiPON interface was discerned in the cross-section image (Figure 9A) and EDS mapping (Figure 9B). EDS line scanning indicates the gradient distribution of N and P across the interface (Figure 9C), which exhibits a multilayer-mosaic structure by HRTEM at different positions (Figure 9D). This methodology will be widely applied to explore the mystery of interface in ASSBs and boost the development of ASSBs by interfacial engineering.

Solid-liquid interfaces

With liquid electrolytes and additives, solid-liquid interfaces are dominant in batteries and determine the ion transfer and reaction kinetics. Such interfaces are of particular importance when soluble reaction

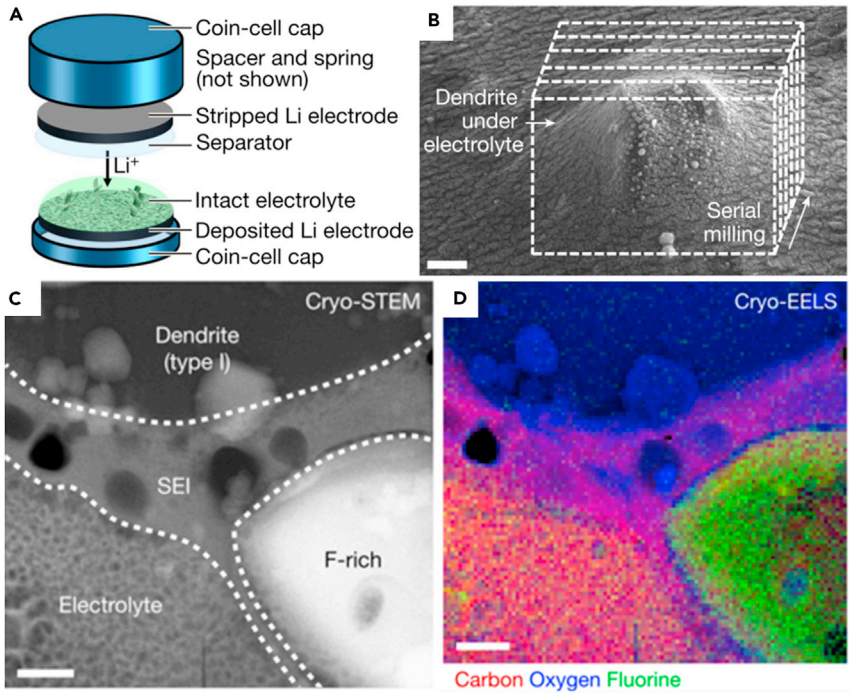

Figure 10. The interface between Li and liquid electrolyte by cryo-FIB and cryo-TEM

(A) Coin-cell setup for Li plating.

(B) The plated Li with electrolyte.

(C and D) Cryo-STEM imaging (C) and its corresponding cryo-EELS elemental mapping (D) (Zachman et al., 2018). Scale bars, 2 μm (B), 300 nm (C and D). Copyright © 2018, Springer Nature.

products, catalysts, or redox mediates are involved, such as flowing active materials, polysulfides, metal ions, and O_2^- radicals. The key to obtaining and imaging such interfaces is to preserve the liquid phase during sample preparation and imaging via cryo treatment. By cryo-FIB and cryo-TEM, Zachman et al.(2018) obtained the interface between Li metal and liquid electrolyte (Figures 10A and 10B) and surprisingly found another kind of dendrite LiH and massive SEI as thick as 200 nm by EELS mapping (Figures 10C and 10D). These results are unprecedented and encourage more efforts on unearthing the treasure behind the various solid-liquid interface in batteries.

CRYO-EM IN THE FUTURE

The successful application of cryo-EM for battery materials and interfaces has achieved many exciting and significant results in the past four years, enriching the fundamental understanding of nano/microstructure and facilitating the development of the battery. Note that there are still lots of unknown structures, unsolved issues, and unclear mechanisms related to the cathode, electrolyte, anode, and their interfaces. Some of the examples are listed in Figure 11 and require cryo-EM to explore their structure and interfaces. For example, the structural nature of the oxidized oxygen anion at the high voltage (Liu et al., 2018c; Yang et al., 2021c), soluble polysulfides (Fan et al., 2021), solvated ions (Yang et al., 2021b; Zhang et al., 2021b), etc. has never been directly visualized. Space charge layer and interfacial reaction present between solid electrolytes and active materials are some of the unsolved issues hindering the fast charge transfer in all-solid-state batteries (Cheng et al., 2020b; Wang et al., 2020a). The working principle of Li plating/stripping and its interplay with SEI is unclear, especially under various operation conditions (Dong et al., 2021a).

Besides the aforementioned solid-solid interface and the solid-liquid interface, the solid-gas interface and even the liquid-gas interface should also be taken into consideration. Gases (e.g., O_2, CO_2, and H_2) are present and involved in the battery reactions, such as O_2 evolution from the oxide cathodes, oxygen cathode, decomposition of electrolytes, and SEI. These gases will be trapped at a low temperature, which enables

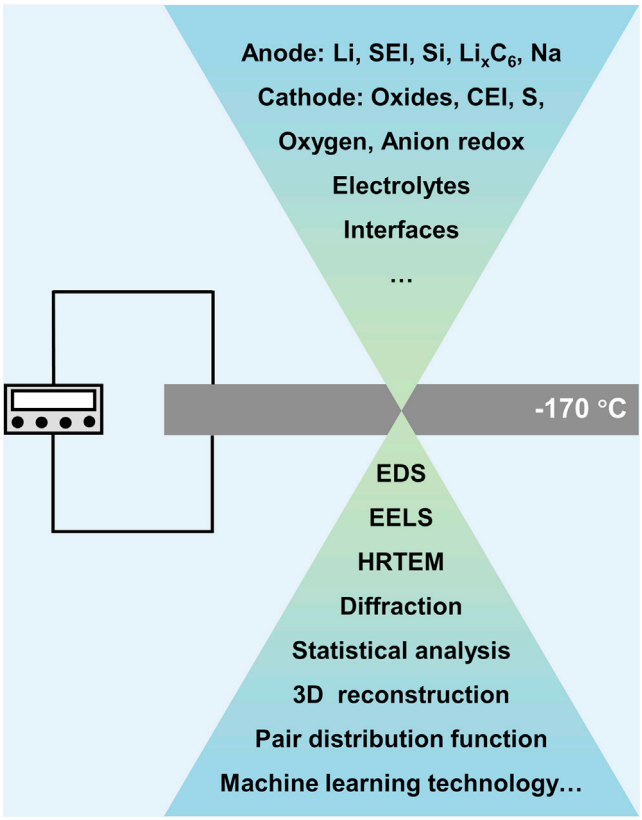

Figure 11. Future cryo-EM for battery materials and interfaces.

the exploration of the related reactions by cryo-EM. For instance, oxygen is a gas at ambient temperature but becomes solid at −218°C, implying that it is possible to study the oxygen release process by cryo-TEM using liquid helium.

The cryo-EM in the future is expected to be more efficient, more integrated, and more intelligent. The development of faster cameras and lower-dose imaging technology helps to obtain a higher signal-to-noise ratio with less damage. In addition, other functions should be integrated with the cryo holder, enabling various *in situ* experiments, such as *in situ* bias and cryo holder, mechanical and cryo holder, and gas and cryo holder. These functional holders will yield many interesting and unprecedented results. We also hope that the emerging technologies can be applied for battery materials and interfaces, such as cryo-micro electron diffraction (cryo-microED), cryo-electron tomography (cryo-ET), cryo-electron diffraction pair distribution function (cryo-ePDF), and machine learning. Cryo-microED can achieve high-spatial-resolution diffraction of samples to obtain various phase distributions at different positions. Cryo-ET and cryo-ePDF are helpful to analyze the amorphous/glass phases inside the battery, such as amorphous Li, SEI, CEI, and Li_xSi alloy (Jasim et al., 2021; Yang et al., 2021d). Besides, statistical analysis is applied for a reliable and representative result. Last but not least, advanced artificial intelligence and machine learning are promising to assist in collecting and analyzing cryo-EM images automatically to obtain a more accurate, more efficient, and more reliable result.

Limitations of study

A detailed description of advanced artificial intelligence and machine learning applied in TEM can be further conducted. In addition, methods to improve the resolution of cryo-EM can be explored.

SUPPLEMENTAL INFORMATION

Supplemental information can be found online at https://doi.org/10.1016/j.isci.2021.103402.

ACKNOWLEDGMENTS

The authors thank the financial supports from the National Natural Science Foundation of China (NSFC No. 22005334 and 21773301) and Natural Science Foundation of Beijing (Grant No. Z200013).

AUTHOR CONTRIBUTIONS

S.W. wrote and revised the manuscript and prepared figures. Y.L. and X.W. conceptualized, wrote, and revised the manuscript.

DECLARATION OF INTERESTS

The authors declare no competing interests.

REFERENCES

Alvarado, J., Schroeder, M.A., Zhang, M., Borodin, O., Gobrogge, E., Olguin, M., Ding, M.S., Gobet, M., Greenbaum, S., Meng, Y.S., and Xu, K. (2018). A carbonate-free, sulfone-based electrolyte for high-voltage Li-ion batteries. Mater. Today *21*, 341–353. https://doi.org/10.1016/j.mattod.2018.02.005.

Alvarado, J., Schroeder, M.A., Pollard, T.P., Wang, X., Lee, J.Z., Zhang, M., Wynn, T., Ding, M., Borodin, O., Meng, Y.S., and Xu, K. (2019). Bisalt ether electrolytes: a pathway towards lithium metal batteries with Ni-rich cathodes. Energy Environ. Sci. *12*, 780–794. https://doi.org/10.1039/c8ee02601g.

Aurbach, D., Ein-Ely, Y., and Zaban, A. (1994). The surface chemistry of lithium electrodes in alkyl carbonate solutions. J. Electrochem. Soc. *141*, L1–L3. https://doi.org/10.1149/1.2054718.

Banerjee, A., Wang, X., Fang, C., Wu, E.A., and Meng, Y.S. (2020). Interfaces and interphases in all-solid-state batteries with inorganic solid electrolytes. Chem. Rev. *120*, 6878–6933. https://doi.org/10.1021/acs.chemrev.0c00101.

Chen, J. (2021). Advanced electron microscopy of nanophased synthetic polymers and soft complexes for energy and medicine applications. Nanomaterials *11*, 2405. https://doi.org/10.3390/nano11092405.

Cheng, D., Wynn, T.A., Wang, X., Wang, S., Zhang, M., Shimizu, R., Bai, S., Nguyen, H., Fang, C., Kim, M.-c., et al. (2020a). Unveiling the stable nature of the solid electrolyte interphase between lithium metal and LiPON via cryogenic electron microscopy. Joule *4*, 2484–2500. https://doi.org/10.1016/j.joule.2020.08.013.

Cheng, Z., Liu, M., Ganapathy, S., Li, C., Li, Z., Zhang, X., He, P., Zhou, H., and Wagemaker, M. (2020b). Revealing the impact of space-charge layers on the Li-ion transport in all-solid-state batteries. Joule *4*, 1311–1323. https://doi.org/10.1016/j.joule.2020.04.002.

Cui, J., Zheng, H., and He, K. (2020). Air-protective Cryo-FIB tomography of sensitive materials for energy applications. Microsc. Microanal. *26*, 1828–1829. https://doi.org/10.1017/s1431927620019522.

Dong, K., Xu, Y., Tan, J., Osenberg, M., Sun, F., Kochovski, Z., Pham, D.T., Mei, S., Hilger, A., Ryan, E., et al. (2021a). Unravelling the mechanism of lithium nucleation and growth and the interaction with the solid electrolyte interface. ACS Energy Lett. *6*, 1719–1728. https://doi.org/10.1021/acsenergylett.1c00551.

Dong, R., Zheng, L., Bai, Y., Ni, Q., Li, Y., Wu, F., Ren, H., and Wu, C. (2021b). Elucidating the mechanism of fast Na storage kinetics in ether electrolytes for hard carbon anodes. Adv. Mater. *33*, 2008810. https://doi.org/10.1002/adma.202008810.

Fan, K., Ying, Y., Luo, X., and Huang, H. (2021). Nitride MXenes as sulfur hosts for thermodynamic and kinetic suppression of polysulfide shuttling: a computational study. J. Mater. Chem. A. https://doi.org/10.1039/D1TA06759A.

Fang, C., Li, J., Zhang, M., Zhang, Y., Yang, F., Lee, J.Z., Lee, M.-H., Alvarado, J., Schroeder, M.A., Yang, Y., et al. (2019). Quantifying inactive lithium in lithium metal batteries. Nature *572*, 511–515. https://doi.org/10.1038/s41586-019-1481-z.

Gao, A., Li, X., Meng, F., Guo, S., Lu, X., Su, D., Wang, X., Zhang, Q., and Gu, L. (2020). In operando visualization of cation disorder unravels voltage decay in Ni-rich cathodes. Small Methods *5*, 2000730. https://doi.org/10.1002/smtd.202000730.

Han, B., Feng, D., Li, S., Zhang, Z., Zou, Y., Gu, M., Meng, H., Wang, C., Xu, K., Zhao, Y., et al. (2020). Self-regulated phenomenon of inorganic artificial solid electrolyte interphase for lithium metal batteries. Nano Lett. *20*, 4029–4037. https://doi.org/10.1021/acs.nanolett.0c01400.

Han, B., Zhang, Z., Zou, Y., Xu, K., Xu, G., Wang, H., Meng, H., Deng, Y., Li, J., and Gu, M. (2021a). Poor stability of Li_2CO_3 in the solid electrolyte interphase of a lithium-metal anode revealed by cryo-electron microscopy. Adv. Mater. *33*, 2100404. https://doi.org/10.1002/adma.202100404.

Han, B., Zou, Y., Xu, G., Hu, S., Kang, Y., Qian, Y., Wu, J., Ma, X., Yao, J., Li, T., et al. (2021b). Additive stabilization of SEI on graphite observed using cryo-electron microscopy. Energy Environ. Sci. *14*, 4882. https://doi.org/10.1039/d1ee01678d.

Han, B., Zou, Y., Zhang, Z., Yang, X., Shi, X., Meng, H., Wang, H., Xu, K., Deng, Y., and Gu, M. (2021c). Probing the Na metal solid electrolyte interphase via cryo-transmission electron microscopy. Nat. Commun. *12*, 3066. https://doi.org/10.1038/s41467-021-23368-6.

He, Y., Jiang, L., Chen, T., Xu, Y., Jia, H., Yi, R., Xue, D., Song, M., Genc, A., Bouchet-Marquis, C., et al. (2021). Progressive growth of the solid-electrolyte interphase towards the Si anode interior causes capacity fading. Nat. Nanotechnol. *16*, 1113–1120. https://doi.org/10.1038/s41565-021-00947-8.

Huang, J., Guo, X., Du, X., Lin, X., Huang, J.-Q., Tan, H., Zhu, Y., and Zhang, B. (2019a). Nanostructures of solid electrolyte interphases and their consequences for microsized Sn anodes in sodium ion batteries. Energy Environ. Sci. *12*, 1550–1557. https://doi.org/10.1039/c8ee03632b.

Huang, W., Attia, P.M., Wang, H., Renfrew, S.E., Jin, N., Das, S., Zhang, Z., Boyle, D.T., Li, Y., Bazant, M.Z., et al. (2019b). Evolution of the solid-electrolyte interphase on carbonaceous anodes visualized by atomic-resolution cryogenic electron microscopy. Nano Lett. *19*, 5140–5148. https://doi.org/10.1021/acs.nanolett.9b01515.

Huang, W., Boyle, D.T., Li, Y., Li, Y., Pei, A., Chen, H., and Cui, Y. (2019c). Nanostructural and electrochemical evolution of the solid-electrolyte interphase on CuO nanowires revealed by cryogenic-electron microscopy and impedance spectroscopy. ACS Nano *13*, 737–744. https://doi.org/10.1021/acsnano.8b08012.

Huang, W., Wang, J., Braun, M.R., Zhang, Z., Li, Y., Boyle, D.T., McIntyre, P.C., and Cui, Y. (2019d). Dynamic structure and chemistry of the silicon solid-electrolyte interphase visualized by cryogenic electron microscopy. Matter *1*, 1232–1245. https://doi.org/10.1016/j.matt.2019.09.020.

Huang, W., Wang, H., Boyle, D.T., Li, Y., and Cui, Y. (2020). Resolving nanoscopic and mesoscopic heterogeneity of fluorinated species in battery solid-electrolyte interphases by cryogenic electron microscopy. ACS Energy Lett. *5*, 1128–1135. https://doi.org/10.1021/acsenergylett.0c00194.

Huang, S., Yang, J., Ma, L., Ding, J., Wang, X., Peng, C., Zhao, B., Cao, M., Zheng, J., Zhang, X.X., and Chen, J. (2021). Effectively regulating more robust amorphous Li clusters for ultrastable dendrite-free cycling. Adv. Sci. *8*, 2101584. https://doi.org/10.1002/advs.202101584.

Ihsan-Ul-Haq, M., Huang, H., Wu, J., Cui, J., Yao, S., Chong, W.G., Huang, B., and Kim, J.-K. (2020). Thin solid electrolyte interface on chemically bonded Sb_2Te_3/CNT composite anodes for high performance sodium ion full cells. Nano Energy *71*, 104613. https://doi.org/10.1016/j.nanoen.2020.104613.

Ihsan-Ul-Haq, M., Cui, J., Mubarak, N., Xu, M., Shen, X., Luo, Z., Huang, B., and Kim, J.-K. (2021a). Revealing cathode-electrolyte interface on flower-shaped $Na_3V_2(PO_4)_3$/C cathode through cryogenic electron microscopy. Adv. Energy Sustain. Res. *2*, 2100072. https://doi.org/10.1002/aesr.202100072.

Ihsan-Ul-Haq, M., Huang, H., Wu, J., Mubarak, N., Susca, A., Luo, Z., Huang, B., and Kim, J.-K. (2021b). Unveiling solid electrolyte interface morphology and electrochemical kinetics of amorphous Sb_2Se_3/CNT composite anodes for ultrafast sodium storage. Carbon *171*, 119–129. https://doi.org/10.1016/j.carbon.2020.09.011.

Jaiser, S., Kumberg, J., Klaver, J., Urai, J.L., Schabel, W., Schmatz, J., and Scharfer, P. (2017). Microstructure formation of lithium-ion battery electrodes during drying-an ex-situ study using cryogenic broad ion beam slope cutting and scanning electron microscopy (Cryo-BIB-SEM). J. Power Sourc. *345*, 97–107. https://doi.org/10.1016/j.jpowsour.2017.01.117.

Jasim, A.M., He, X., Xing, Y., White, T.A., and Young, M.J. (2021). Cryo-ePDF: overcoming electron beam damage to study the local atomic structure of amorphous ALD aluminum oxide thin films within a TEM. ACS Omega *6*, 8986–9000. https://doi.org/10.1021/acsomega.0c06124.

Jin, C., Liu, T., Sheng, O., Li, M., Liu, T., Yuan, Y., Nai, J., Ju, Z., Zhang, W., Liu, Y., et al. (2021). Rejuvenating dead lithium supply in lithium metal anodes by iodine redox. Nat. Energy *6*, 378–387. https://doi.org/10.1038/s41560-021-00789-7.

Ju, Z., Nai, J., Wang, Y., Liu, T., Zheng, J., Yuan, H., Sheng, O., Jin, C., Zhang, W., Jin, Z., et al. (2020). Biomacromolecules enabled dendrite-free lithium metal battery and its origin revealed by cryo-electron microscopy. Nat. Commun. *11*, 488. https://doi.org/10.1038/s41467-020-14358-1.

Ju, Z., Tao, X., Jin, C., Yuan, H., Yang, T., Sheng, O., Liu, T., Liu, Y., Wang, Y., Ma, F., et al. (2021a). A fast-ion conducting interface enabled by aluminum silicate fibers for stable Li metal batteries. Chem. Eng. J. *408*, 128016. https://doi.org/10.1016/j.cej.2020.128016.

Ju, Z., Yuan, H., Sheng, O., Liu, T., Nai, J., Wang, Y., Liu, Y., and Tao, X. (2021b). Cryo-electron microscopy for unveiling the sensitive battery materials. Small Sci. 2100055. https://doi.org/10.1002/smsc.202100055.

Le, P.M.L., Vo, T.D., Pan, H., Jin, Y., He, Y., Cao, X., Nguyen, H.V., Engelhard, M.H., Wang, C., Xiao, J., and Zhang, J.-G. (2020). Excellent cycling stability of sodium anode enabled by a stable solid electrolyte interphase formed in ether-based electrolytes. Adv. Funct. Mater. *30*, 2001151. https://doi.org/10.1002/adfm.202001151.

Lee, J.Z., Wynn, T.A., Schroeder, M.A., Alvarado, J., Wang, X., Xu, K., and Meng, Y.S. (2019). Cryogenic focused ion beam characterization of lithium metal anodes. ACS Energy Lett. *4*, 489–493. https://doi.org/10.1021/acsenergylett.8b02381.

Levin, B.D.A., Zachman, M.J., Werner, J.G., Sahore, R., Nguyen, K.X., Han, Y., Xie, B., Ma, L., Archer, L.A., Giannelis, E.P., et al. (2017). Characterization of sulfur and nanostructured sulfur battery cathodes in electron microscopy without sublimation artifacts. Microsc. Microanal. *23*, 155–162. https://doi.org/10.1017/s1431927617000058.

Li, Y., Li, Y., Pei, A., Yan, K., Sun, Y., Wu, C.-L., Joubert, L.-M., Chin, R., Koh, A.L., Yu, Y., et al. (2017). Atomic structure of sensitive battery materials and Interfaces revealed by cryo-electron microscopy. Science *358*, 506–510. https://doi.org/10.1126/science.aam6014.

Li, Y., Huang, W., Li, Y., Pei, A., Boyle, D.T., and Cui, Y. (2018). Correlating structure and function of battery interphases at atomic resolution using cryoelectron microscopy. Joule *2*, 2167–2177. https://doi.org/10.1016/j.joule.2018.08.004.

Li, Y., Huang, W., Li, Y., Chiu, W., and Cui, Y. (2020a). Opportunities for cryogenic electron microscopy in materials science and nanoscience. ACS Nano *14*, 9263–9276. https://doi.org/10.1021/acsnano.0c05020.

Li, Y., Wang, X., Zhou, H., Xing, X., Banerjee, A., Holoubek, J., Liu, H., Meng, Y.S., and Liu, P. (2020b). Thin solid electrolyte layers enabled by nanoscopic polymer binding. ACS Energy Lett. *5*, 955–961. https://doi.org/10.1021/acsenergylett.0c00040.

Li, S., Zhang, S., Chai, S., Zang, X., Cheng, C., Ma, F., Zhang, L., and Lu, Y. (2021). Structured solid electrolyte interphase enable reversible Li electrodeposition in flame-retardant phosphate-based electrolyte. Energy Storage Mater. *42*, 628–635. https://doi.org/10.1016/j.ensm.2021.08.015.

Lin, D.C., Liu, Y.Y., and Cui, Y. (2017). Reviving the lithium metal anode for high-energy batteries. Nat. Nanotechnol. *12*, 194–206. https://doi.org/10.1038/nnano.2017.16.

Lin, D., Liu, Y., Li, Y., Li, Y., Pei, A., Xie, J., Huang, W., and Cui, Y. (2019). Fast galvanic lithium corrosion involving a Kirkendall-type mechanism. Nat. Chem. *11*, 382–389. https://doi.org/10.1038/s41557-018-0203-8.

Liu, B., Zhang, J.-G., and Xu, W. (2018a). Advancing lithium metal batteries. Joule *2*, 833–845. https://doi.org/10.1016/j.joule.2018.03.008.

Liu, H., Wang, X., Zhou, H., Lim, H.-D., Xing, X., Yan, Q., Meng, Y.S., and Liu, P. (2018b). Structure and solution dynamics of lithium methyl carbonate as a protective layer for lithium metal. ACS Appl. Energy Mater. *1*, 1864–1869. https://doi.org/10.1021/acsaem.8b00348.

Liu, S., Liu, Z., Shen, X., Li, W., Gao, Y., Banis, M.N., Li, M., Chen, K., Zhu, L., Yu, R., et al. (2018c). Surface doping to enhance structural integrity and performance of Li-rich layered oxide. Adv. Energy Mater. *8*, 1802105. https://doi.org/10.1002/aenm.201802105.

Liu, X.-C., Yang, Y., Wu, J., Liu, M., Zhou, S.P., Levi, B.D.A., Zhou, X.-D., Cong, H., Muller, D.A., Ajayan, P.M., et al. (2018d). Dynamic hosts for high-performance Li-S batteries studied by cryogenic transmission electron microscopy and in situ X-ray diffraction. ACS Energy Lett. *3*, 1325–1330. https://doi.org/10.1021/acsenergylett.8b00561.

Liu, Y., Lin, D., Li, Y., Chen, G., Pei, A., Nix, O., Li, Y., and Cui, Y. (2018e). Solubility-mediated sustained release enabling nitrate additive in carbonate electrolytes for stable lithium metal anode. Nat. Commun. *9*, 3656. https://doi.org/10.1038/s41467-018-06077-5.

Liu, J., Bao, Z., Cui, Y., Dufek, E.J., Goodenough, J.B., Khalifah, P., Li, Q., Liaw, B.Y., Liu, P., Manthiram, A., et al. (2019a). Pathways for practical high-energy long-cycling lithium metal batteries. Nat. Energy *4*, 180–186. https://doi.org/10.1038/s41560-019-0338-x.

Liu, Y., Zhu, Y., and Cui, Y. (2019b). Challenges and opportunities towards fast-charging battery materials. Nat. Energy *4*, 540–550. https://doi.org/10.1038/s41560-019-0405-3.

Liu, T., Zheng, J., Hu, H., Sheng, O., Ju, Z., Lu, G., Liu, Y., Nai, J., Wang, Y., Zhang, W., and Tao, X. (2021a). In-situ construction of a Mg-modified interface to guide uniform lithium deposition for stable all-solid-state batteries. J. Energy Chem. *55*, 272–278. https://doi.org/10.1016/j.jechem.2020.07.009.

Liu, Y., Ju, Z., Zhang, B., Wang, Y., Nai, J., Liu, T., and Tao, X. (2021b). Visualizing the sensitive lithium with atomic precision: cryogenic electron microscopy for batteries. Acc. Chem. Res. *54*, 2088–2099. https://doi.org/10.1021/acs.accounts.1c00120.

Liu, Y., Wu, Y., Zheng, J., Wang, Y., Ju, Z., Lu, G., Sheng, O., Nai, J., Liu, T., Zhang, W., and Tao, X. (2021c). Silicious nanowires enabled dendrites suppression and flame retardancy for advanced lithium metal anodes. Nano Energy *82*, 105723. https://doi.org/10.1016/j.nanoen.2020.105723.

Mubarak, N., Rehman, F., Wu, J., Ihsan-Ul-Haq, M., Li, Y., Zhao, Y., Shen, X., Luo, Z., Huang, B., and Kim, J.-K. (2021). Morphology, chemistry, performance trident: insights from hollow, mesoporous carbon nanofibers for dendrite-free sodium metal batteries. Nano Energy *86*, 106132. https://doi.org/10.1016/j.nanoen.2021.106132.

Peled, E., Golodnitsky, D., and Ardel, G. (1997). Advanced model for solid electrolyte interphase electrodes in liquid and polymer electrolytes. J. Electrochem. Soc. *144*, L208–L210. https://doi.org/10.1149/1.1837858.

Ren, X.-C., Zhang, X.-Q., Xu, R., Huang, J.-Q., and Zhang, Q. (2020). Analyzing energy materials by cryogenic electron microscopy. Adv. Mater. *32*, 1908293. https://doi.org/10.1002/adma.201908293.

Sheng, O., Jin, C., Chen, M., Ju, Z., Liu, Y., Wang, Y., Nai, J., Liu, T., Zhang, W., and Tao, X. (2020a). Platinum nano-interlayer enhanced interface for stable all-solid-state batteries observed via cryo-transmission electron microscopy. J. Mater. Chem. A. *8*, 13541–13547. https://doi.org/10.1039/d0ta03270k.

Sheng, O., Zheng, J., Ju, Z., Jin, C., Wang, Y., Chen, M., Nai, J., Liu, T., Zhang, W., Liu, Y., and Tao, X. (2020b). In situ construction of a LiF-enriched interface for stable all-solid-state batteries and its origin revealed by cryo-TEM. Adv. Mater. *32*, 2000223. https://doi.org/10.1002/adma.202000223.

Song, Y.B., Kim, D.H., Kwak, H., Han, D., Kang, S., Lee, J.H., Bak, S.-M., Nam, K.-W., Lee, H.-W., and

Jung, Y.S. (2020). Tailoring solution-processable Li argyrodites $Li_{6+x}P_{1-x}M_xS_5I$ (M = Ge, Sn) and their microstructural evolution revealed by cryo-TEM for all-solid-state batteries. Nano Lett. *20*, 4337–4345. https://doi.org/10.1021/acs.nanolett.0c01028.

Soulmi, N., Dambournet, D., Rizzi, C., Sirieix-Plenet, J., Duttine, M., Wattiaux, A., Swiatowska, J., Borkiewicz, O.J., Groult, H., and Gaillon, L. (2017). Structural and morphological description of Sn/SnO_x core-shell nanoparticles synthesized and isolated from ionic liquid. Inorg. Chem. *56*, 10099–10106. https://doi.org/10.1021/acs.inorgchem.7b01850.

Sun, H., Zhu, G., Xu, X., Liao, M., Li, Y.Y., Angell, M., Gu, M., Zhu, Y., Hung, W.H., Li, J., et al. (2019). A safe and non-flammable sodium metal battery based on an ionic liquid electrolyte. Nat. Commun. *10*, 3302. https://doi.org/10.1038/s41467-019-11102-2.

Thenuwara, A.C., Shetty, P.P., and McDowell, M.T. (2019). Distinct nanoscale interphases and morphology of lithium metal electrodes operating at low temperatures. Nano Lett. *19*, 8664–8672. https://doi.org/10.1021/acs.nanolett.9b03330.

Tyukalova, E., Vimal Vas, J., Ignatans, R., Mueller, A.D., Medwal, R., Imamura, M., Asada, H., Fukuma, Y., Rawat, R.S., Tileli, V., and Duchamp, M. (2021). Challenges and applications to operando and in situ TEM imaging and spectroscopic capabilities in a cryogenic temperature range. Acc. Chem. Res. *54*, 3125–3135. https://doi.org/10.1021/acs.accounts.1c00078.

Verma, P., Maire, P., and Novák, P. (2010). A review of the features and analyses of the solid electrolyte interphase in Li-ion batteries. Electrochim. Acta *55*, 6332–6341. https://doi.org/10.1016/j.electacta.2010.05.072.

Vilá, R.A., Huang, W., and Cui, Y. (2020). Nickel impurities in the solid-electrolyte interphase of lithium-metal anodes revealed by cryogenic electron microscopy. Cell Rep. Phys. Sci. *1*, 100188. https://doi.org/10.1016/j.xcrp.2020.100188.

Wang, X., Zhang, M., Alvarado, J., Wang, S., Sina, M., Lu, B., Bouwer, J., Xu, W., Xiao, J., Zhang, J.-G., et al. (2017). New insights on the structure of electrochemically deposited lithium metal and its solid electrolyte interphases via cryogenic TEM. Nano Lett. *17*, 7606–7612. https://doi.org/10.1021/acs.nanolett.7b03606.

Wang, X., Li, Y., and Meng, Y.S. (2018). Cryogenic electron microscopy for characterizing and diagnosing batteries. Joule *2*, 2225–2234. https://doi.org/10.1016/j.joule.2018.10.005.

Wang, H., Li, Y., Li, Y., Liu, Y., Lin, D., Zhu, C., Chen, G., Yang, A., Yan, K., Chen, H., et al. (2019a). Wrinkled graphene cages as hosts for high-capacity Li metal anodes shown by cryogenic electron microscopy. Nano Lett. *19*, 1326–1335. https://doi.org/10.1021/acs.nanolett.8b04906.

Wang, J., Huang, W., Pei, A., Li, Y., Shi, F., Yu, X., and Cui, Y. (2019b). Improving cyclability of Li metal batteries at elevated temperatures and its origin revealed by cryo-electron microscopy. Nat. Energy *4*, 664–670. https://doi.org/10.1038/s41560-019-0413-3.

Wang, L., Xie, R., Chen, B., Yu, X., Ma, J., Li, C., Hu, Z., Sun, X., Xu, C., Dong, S., et al. (2020a). In-situ visualization of the space-charge-layer effect on interfacial lithium-ion transport in all-solid-state batteries. Nat. Commun. *11*, 5889. https://doi.org/10.1038/s41467-020-19726-5.

Wang, X., Pawar, G., Li, Y., Ren, X., Zhang, M., Lu, B., Banerjee, A., Liu, P., Dufek, E.J., Zhang, J.-G., et al. (2020b). Glassy Li metal anode for high-performance rechargeable Li batteries. Nat. Mater. *19*, 1339–1345. https://doi.org/10.1038/s41563-020-0729-1.

Wu, H., Jia, H., Wang, C., Zhang, J.G., and Xu, W. (2020). Recent progress in understanding solid electrolyte interphase on lithium metal anodes. Adv. Energy Mater. *11*, 2003092. https://doi.org/10.1002/aenm.202003092.

Wu, J., Ihsan-Ul-Haq, M., Chen, Y., and Kim, J.-K. (2021). Understanding solid electrolyte interphases: advanced characterization techniques and theoretical simulations. Nano Energy *89*, 106489. https://doi.org/10.1016/j.nanoen.2021.106489.

Xin, S., You, Y., Wang, S., Gao, H.-C., Yin, Y.-X., and Guo, Y.-G. (2017). Solid-state lithium metal batteries promoted by nanotechnology: progress and prospects. ACS Energy Lett. *2*, 1385–1394. https://doi.org/10.1021/acsenergylett.7b00175.

Xing, X., Li, Y., Wang, X., Petrova, V., Liu, H., and Liu, P. (2019). Cathode electrolyte interface enabling stable Li-S batteries. Energy Storage Mater. *21*, 474–480. https://doi.org/10.1016/j.ensm.2019.06.022.

Xu, Y., Wu, H., He, Y., Chen, Q., Zhang, J.G., Xu, W., and Wang, C. (2020a). Atomic to nanoscale origin of vinylene carbonate enhanced cycling stability of lithium metal anode revealed by cryo-transmission electron microscopy. Nano Lett. *20*, 418–425. https://doi.org/10.1021/acs.nanolett.9b04111.

Xu, Y., Wu, H., Jia, H., Zhang, J.-G., Xu, W., and Wang, C. (2020b). Current density regulated atomic to nanoscale process on Li deposition and solid electrolyte interphase revealed by cryogenic transmission electron microscopy. ACS Nano *14*, 8766–8775. https://doi.org/10.1021/acsnano.0c03344.

Yan, K., Wang, J., Zhao, S., Zhou, D., Sun, B., Cui, Y., and Wang, G. (2019). Temperature-dependent nucleation and growth of dendrite-free lithium metal anodes. Angew. Chem. Int. Ed. *58*, 11364–11368. https://doi.org/10.1002/anie.201905251.

Yang, G., Liu, Z., Weng, S., Zhang, Q., Wang, X., Wang, Z., Gu, L., and Chen, L. (2021a). Iron carbide allured lithium metal storage in carbon nanotube cavities. Energy Storage Mater. *36*, 459–465. https://doi.org/10.1016/j.ensm.2021.01.022.

Yang, G., Zhang, S., Weng, S., Li, X., Wang, X., Wang, Z., and Chen, L. (2021b). Anionic effect on enhancing the stability of a solid electrolyte interphase film for lithium deposition on graphite. Nano Lett. *21*, 5316–5323. https://doi.org/10.1021/acs.nanolett.1c01436.

Yang, L., Liu, Z., Shen, X., Li, S., Hu, Z., Kong, Q., Ma, J., Li, J., Lin, H.-J., Chen, C.-T., et al. (2021c). Effect of vacancy-tailored Mn^{3+} spinning on enhancing structural stability. Energy Storage Mater. https://doi.org/10.1016/j.ensm.2021.10.024.

Yang, Y., Zhou, J., Zhu, F., Yuan, Y., Chang, D.J., Kim, D.S., Pham, M., Rana, A., Tian, X., Yao, Y., et al. (2021d). Determining the three-dimensional atomic structure of an amorphous solid. Nature *592*, 60–64. https://doi.org/10.1038/s41586-021-03354-0.

Yu, S.-H., Zachman, M.J., Kang, K., Gao, H., Huang, X., DiSalvo, F.J., Park, J., Kourkoutis, L.F., and Abruna, H.D. (2019). Atomic-scale visualization of electrochemical lithiation processes in monolayer MoS_2 by cryogenic electron microscopy. Adv. Energy Mater. *9*, 1902773. https://doi.org/10.1002/aenm.201902773.

Yuan, H., Nai, J., Fang, Y., Lu, G., Tao, X., and Lou, X.W.D. (2020a). Double-shelled C@MoS2 structures preloaded with sulfur: an additive reservoir for stable lithium metal anodes. Angew. Chem. Int. Ed. *59*, 15839–15843. https://doi.org/10.1002/anie.202001989.

Yuan, H., Nai, J., Tian, H., Ju, Z., Zhang, W., Liu, Y., Tao, X., and Lou, X.W. (2020b). An ultrastable lithium metal anode enabled by designed metal fluoride spansules. Sci. Adv. *6*, eaaz3112. https://doi.org/10.1126/sciadv.aaz3112.

Yuan, S., Weng, S., Wang, F., Dong, X., Wang, Y., Wang, Z., Shen, C., Bao, J.L., Wang, X., and Xia, Y. (2021). Revisiting the designing criteria of advanced solid electrolyte interphase on lithium metal anode under practical condition. Nano Energy *83*, 105847. https://doi.org/10.1016/j.nanoen.2021.105847.

Zachman, M.J., Tu, Z., Choudhury, S., Archer, L.A., and Kourkoutis, L.F. (2018). Cryo-STEM mapping of solid-liquid interfaces and dendrites in lithium-metal batteries. Nature *560*, 345–349. https://doi.org/10.1038/s41586-018-0397-3.

Zachman, M.J., Tu, Z., Archer, L.A., and Kourkoutis, L.F. (2020). Nanoscale elemental mapping of intact solid-liquid interfaces and reactive materials in energy devices enabled by cryo-FIB/SEM. ACS Energy Lett. *5*, 1224–1232. https://doi.org/10.1021/acsenergylett.0c00202.

Zhang, N., Levin, B.D.A., Yang, Y., Muller, D.A., and Abruna, H.D. (2018). Porous Fe_3O_4 nanospheres as effective sulfur hosts for Li-S batteries. J. Electrochem. Soc. *165*, A1656–A1661. https://doi.org/10.1149/2.0691809jes.

Zhang, N., Yang, Y., Feng, X., Yu, S.-H., Seok, J., Muller, D.A., and Abruna, H.D. (2019). Sulfur encapsulation by MOF-derived CoS_2 embedded in carbon hosts for high-performance Li-S batteries. J. Mater. Chem. A. *7*, 21128–21139. https://doi.org/10.1039/c9ta06947j.

Zhang, B., Shi, H., Ju, Z., Huang, K., Lian, C., Wang, Y., Sheng, O., Zheng, J., Nai, J., Liu, T., et al. (2020a). Arrayed silk fibroin for high-performance Li metal batteries and atomic interface structure revealed by cryo-TEM. J. Mater. Chem. A. *8*, 26045–26054. https://doi.org/10.1039/d0ta09753e.

Zhang, C., Feng, Y., Han, Z., Gao, S., Wang, M., and Wang, P. (2020b). Electrochemical and structural analysis in all-solid-state lithium batteries by analytical electron microscopy: progress and perspectives. Adv. Mater. *32*, 1903747. https://doi.org/10.1002/adma.201903747.

Zhang, K., Wu, F., Zhang, K., Weng, S., Wang, X., Gao, M., Sun, Y., Cao, D., Bai, Y., Xu, H., et al. (2021a). Chlorinated dual-protective layers as interfacial stabilizer for dendrite-free lithium metal anode. Energy Storage Mater. *41*, 485–494. https://doi.org/10.1016/j.ensm.2021.06.023.

Zhang, S., Yang, G., Liu, Z., Li, X., Wang, X., Chen, R., Wu, F., Wang, Z., and Chen, L. (2021b). Competitive solvation enhanced stability of lithium metal anode in dual-salt electrolyte. Nano Lett. *21*, 3310–3317. https://doi.org/10.1021/acs.nanolett.1c00848.

Zhang, Z., Cui, Y., Vila, R., Li, Y., Zhang, W., Zhou, W., Chiu, W., and Cui, Y. (2021c). Cryogenic electron microscopy for energy materials. Acc. Chem. Res. *54*, 3505–3517. https://doi.org/10.1021/acs.accounts.1c00183.

Zhang, Z., Yang, J., Huang, W., Wang, H., Zhou, W., Li, Y., Li, Y., Xu, J., Huang, W., Chiu, W., and Cui, Y. (2021d). Cathode-electrolyte interphase in lithium batteries revealed by cryogenic electron microscopy. Matter *4*, 302–312. https://doi.org/10.1016/j.matt.2020.10.021.

Zheng, H., Cui, J., and He, K. (2020). A new cryo-FIB-TEM approach for damage-free characterization of garnet electrolytes in solid-state batteries. Microsc. Microanal. *26*, 2784–2785. https://doi.org/10.1017/s1431927620022783.